



# Mass Optimization of Crane Box Girder Considering Both Ribs and Diaphragms using APDL

Yangzhi Ren<sup>1</sup> · Xuechun Liu<sup>1</sup> · Bin Wang<sup>2</sup>

Received: 31 October 2023 / Accepted: 6 May 2024 / Published online: 10 May 2024  
© Korean Society of Steel Construction 2024

## Abstract

Mass optimization of crane box girder considering both ribs and diaphragms is a crucial aspect of crane structural design in mechanical engineering. However, two common challenges often obscure this process: the sizing of stiffeners such as diaphragms and ribs, and the selection of constraints on state variables related to stresses and deformations for various load cases. In response, this paper focuses on optimizing the dimensions, number, and placement of stiffeners, including ribs and diaphragms, in a two-girder overhead crane structure. The paper begins by establishing criteria for the initial height of the box girder through a comparative analysis of structural strength and stiffness. Subsequently, dimensional relationships between stiffeners and the girder section are built in accordance with the principles of local plate stability. Following this, the ANSYS Parametric Design Language (APDL) program is coded and executed to optimize the crane mass using three methods: sub-problem approximation, sweep, and first-order methods via Module Design OPT for four chosen sets of state variables. A comparative analysis of the optimum crane mass, based on the rounded-up design variables, reveals that constraints on stresses and deformations from both vertical and transversal impact cases, as well as the vertical frequency from dynamic vibration cases, yield the best results. Furthermore, the proposed APDL method is compared and validated against Grey Wolf Optimizer, Whale Optimization Algorithm, Particle Swarm Optimization, and Genetic Algorithm. Finally, a parametric study is conducted using curves and tables to explore the influence of structural stiffness and material property on the optimized dimensions of the girder and stiffeners, as well as the overall mass and mechanical performance.

**Keywords** Mass optimization · Lightweight · Crane girder · Ribs · Diaphragms · APDL

## 1 Introduction

The application of optimization technology holds significant promise in reducing the mass of overhead cranes, thereby effectively saving production time and costs. Typically, the mass of the girder comprises 50% of the load capacity for bridge cranes and 60% for gantry cranes. Therefore, reducing the mass of these girders is essential for lowering expenses and minimizing energy consumption. Consequently, mass optimization stands as a top priority in the structural design of cranes.

DEMAG, a European crane company, has successfully reduced the mass of overhead cranes with a load capacity lower than 50 tons by 15% through the inclusion of girder ribs (Cheng et al., 2012). However, for cranes exceeding 50 tons, mass reduction remains a formidable challenge. In China, the development of lightweight cranes has faced difficulties due to concerns about the reliability and safety of optimized design, even when structural stiffness and strength comply with mandatory regulations (Wan et al., 2008; Wang et al., 2013). Consequently, the practical implementation of mass optimization remains elusive.

Crane mass optimization involves a systematic process in which the dimensions of the girder cross-section (design variables) are optimized while adhering to specific constraints related to structural performance (state variables). The key question is how to ensure both the reliability and safety of mass optimization, which is crucial for its practical application. Early research efforts have centered on the

✉ Yangzhi Ren  
renyz@bjut.edu.cn

<sup>1</sup> College of Architecture and Civil Engineering, Beijing University of Technology, Beijing 100124, China

<sup>2</sup> College of Engineering, Design and Physical Sciences, Brunel University, London, Uxbridge UB8 3PH, UK

selection of design variables and state variables, categorizing them into those with and without stiffeners.

For design variables without stiffeners, Deng et al. (2020) identified web height, flange width, and plate thickness as design variables based on sensitivity analysis of cross-sectional parameters to stress and deformation. Consequently, the dimensions of the girder cross-section are naturally considered design variables, while those of stiffeners are commonly neglected due to their lower sensitivity (Hao et al., 2017; Hou et al., 2018; Li et al., 2020; Qiu et al., 2019; Zhang et al., 2019).

In contrast, for design variables with stiffeners, Savkovic et al. (2017) introduced web local stability as a constraint and achieved a 16% reduction in crane mass. Abid et al. (2015) optimized the shape, number, and location of ribs before optimizing the girder cross-section, resulting in the minimum crane mass. Pavloviu et al. (2017) included local stability constraints for both the web and flange, leading to a 27% reduction in crane mass. Zhang et al. (2021) achieved a 7% reduction in crane mass by designing ribs asymmetrically relative to the centroid axis, adjusting the distance between adjacent ribs on the main web, and offsetting the diaphragm hole. Khoury et al., (2014, 2016) focused on rib optimization and determined the best locations at 1/3 and 1/4 of the web height for curved box girder ribs. Fu et al. (2013) reduced crane mass by 136 kg by decreasing the number of diaphragms from 15 to 10.

In terms of state variables, they encompass stresses, deformations, or frequency for specific cases, and constraints on these variables define the allowable range for design variable changing. Commonly used constraints include normal bending stress on the bottom flange, shear stress on the end plate, and vertical deformation at mid-span (Alhorani, 2020; Li et al., 2018; Pervan et al., 2020). Additionally, Jarmia et al. (2021) introduced constraints on the local stability of the web and flange, while Qi et al. (2021a) considered fatigue strength and overall stability. Patel et al. (2020) examined the main stress, Qi et al. (2021b) the compound stress, Kovacs and Farkas (2017)

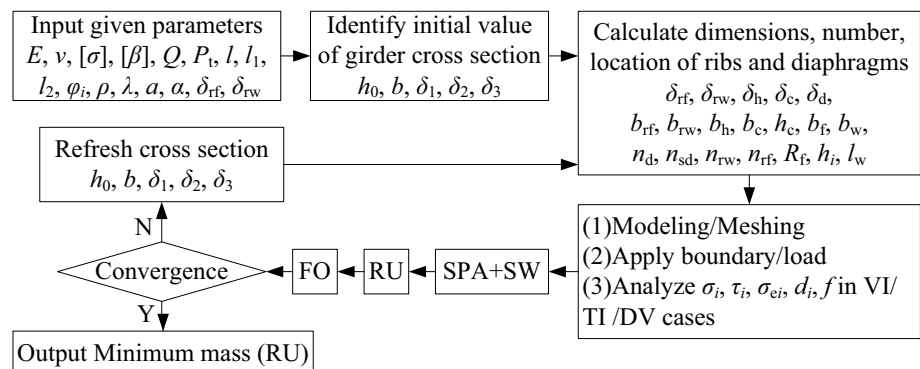
the fillet weld between the girder and diaphragm, and Tong et al. (2013) frequency and energy.

An extensive examination of the existing literature highlights the tendency to either overlook or treat stiffeners separately from the girder cross-section in the process of crane optimization. Additionally, the process of selecting state variables often lacks substantial supporting evidence for specific choices. These two issues together pose a significant challenge to the reliability and safety of crane optimization, which therefore prompts the author to take strides in advancing crane optimization technology. Accordingly, the objective of paper is to identify the optimization process of crane steel box girder considering the iteration of dimension, number and location of stiffeners such as intermediate diaphragms and ribs, and simultaneously to identify the proper constraints on state variables, such as stress, deformation and frequency in optimization process. To do it, the central focus lies in establishing the relationship between stiffeners and girder cross section, followed by the development of four possible optimization models from three load cases. After that, three methods, sub-problem approximation (Zhang et al., 2010), sweep (Pang et al., 2011) and first-order (Hidekazu, 2002), are harnessed to drive mass reduction by programming in the form of ANSYS Parametric Design Language (APDL) coding. Subsequently, optimized solutions are obtained, encompassing the rounded-up dimensions, stress, deformation and frequency levels, which are further compared and validated against Grey Wolf Optimizer, Whale Optimization Algorithm, Particle Swarm Optimization, and Genetic Algorithm (Su et al., 2022). Lastly, a series of parameter studies are conducted to delve into the effect of structural stiffness and material property on the optimized crane mass, dimensions, and mechanical performance.

## 2 Optimization Framework

As illustrated in Fig. 1, the whole optimization process includes (1) Preparing the given parameters related to structural materials and mechanical properties, allowable

Fig. 1 Optimization framework for crane structural design



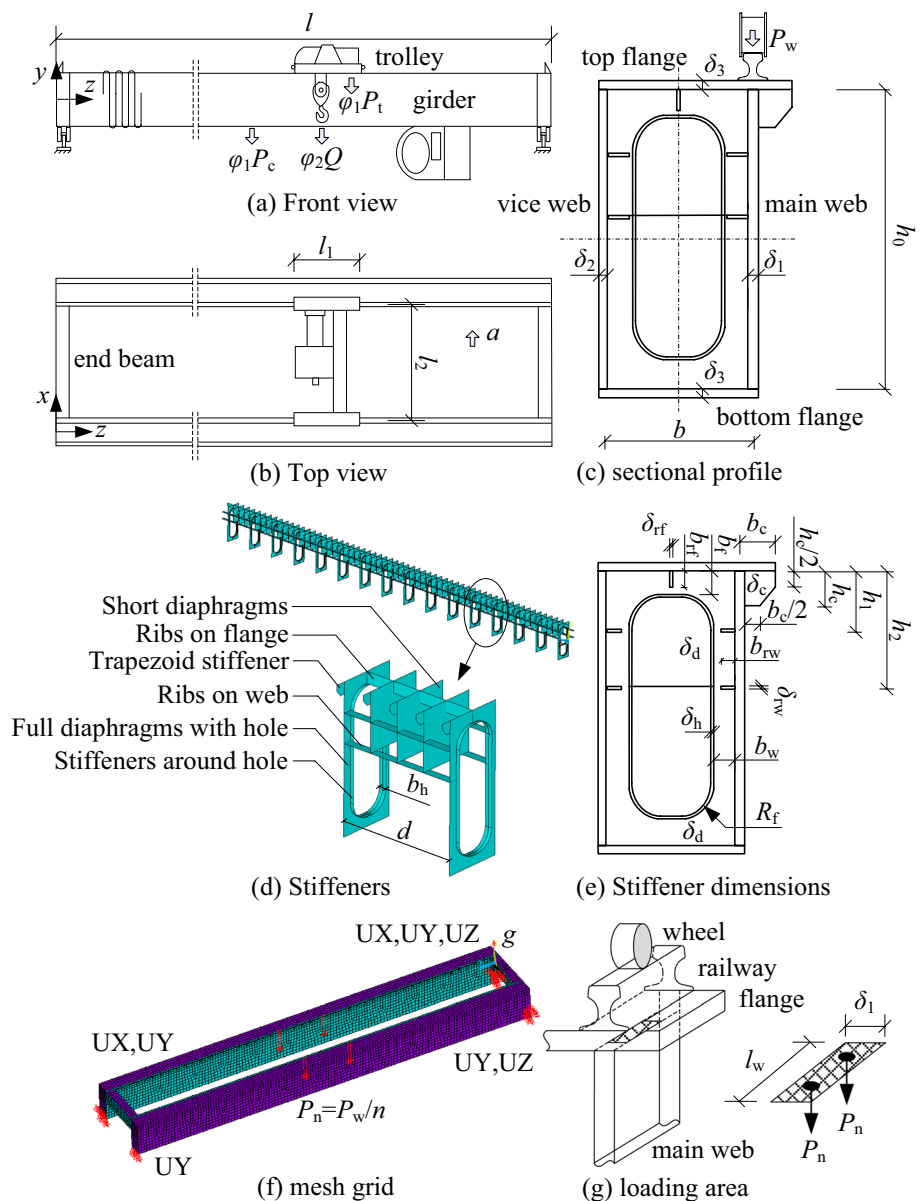
limitation for stresses and deformations, crane dimensions as a whole, trolley mass, rib thickness, (2) Identifying initial values for basic dimensions of girder cross-sections, designated as design variables, (3) Calculating the dimensions of stiffeners, designated as dependant variables, such as ribs and diaphragms based on relationships between girder section and stiffeners, (4) Modeling and meshing the crane girder structure, then analyzing the structural stresses, deformations or frequency in certain load cases, taking them as state variables, and making boundary constraints on them for further optimization, (5) Taking total crane mass as objective function, then optimizing using sub-problem approximation (SPA), sweeping (SW) and first-order (FO) in turn, until termination comes. Note that all above steps are programmed in the form of ANSYS Parametric Design Language (APDL)

code. Following the framework in Fig. 1, given parameters, design variables, dependant variables, constraints on state variables and optimization method will be specified in the following sub-sections, respectively.

### 2.1 Given Parameters

Given parameters refer to the variables provided as background for certain crane structure and loading conditions. As shown in Fig. 2a, consider an overhead crane with loading capacity  $Q$  being 100t. The girder span ( $l$ ) is 25 m, and the mass of the trolley ( $P_t$ ) is calculated as  $0.35Q$ . Correspondingly, to hold the load  $Q$ , the distance  $l_1$  between trolley wheels in longitudinal direction correspondingly sets 2.92 m, and  $l_2$  between trolley rails in transverse direction does 3 m (Fig. 2b).

Fig. 2 Crane structure, dimensions and meshing condition



The girder and stiffeners are made of carbon structural steel with yielding stress  $\sigma_s$  235 MPa and safety coefficient  $n$  1.48, producing allowable normal stress  $[\sigma]$  158.78 MPa. Besides, the deformations in vertical and transverse directions are constrained by applying stiffness coefficients  $[\beta]$  and  $[\beta_t]$  with the values of 500 and 2000, respectively.

Subsequently, material property includes Young’s modulus  $E$  2.06GPa, Poisson’s ratio  $\nu$  0.3 and density  $\rho_c$  7850 kg/m<sup>3</sup>. Two load cases, vertical impact case (VI) and transverse impact case (TI), are considered in which the stress or deformation are chosen as design variables. In VI case, additional coefficient  $\varphi_1$  induced by sudden hoisting or braking goods takes commonly 1.1 as amplification on girder mass  $P_c$  and trolley  $P_t$ , while  $\varphi_2$  does 1.21 for goods weight  $Q$ . In TI case, acceleration  $a$  takes 0.25 m/s<sup>2</sup>. Correspondingly, coefficient  $\varphi_5$  induced by unstable trolley running does 1.5.

Furthermore, to obtain the initial value of cross section for box girder, several ratios are estimated empirically, including the ratio of total stiffener masses to girder  $\alpha$  1/3, and the ratio of all electrical equipment masses to girder  $\lambda$  0.2. Besides, the summation of thicknesses  $\delta$  for both main and vice webs takes 16 mm, in which main web thickness  $\delta_1$  does 8 mm. The thicknesses  $\delta_{tr}$ ,  $\delta_{rw}$  for ribs on webs and flanges take uniform 6 mm.

### 2.2 Design Variables

In mass optimization of crane box girder, design variables refer to five dimensions of girder section, such as the net web height  $h_0$ , width of flanges  $b$  measured by two web mid-lines, thicknesses of main web, vice web and flanges  $\delta_1, \delta_2, \delta_3$  (Fig. 2c). Main web refers to the web burdening trolley railway on top flange. In optimization model, constraints on design variables are issued as  $1.5 \text{ m} \leq h_0 \leq 2.5 \text{ m}$ ,  $0.5 \text{ m} \leq b \leq 1.5 \text{ m}$ ,  $6 \text{ mm} \leq \delta_i \leq 20 \text{ mm}$  ( $i=1,2,3$ ).

To begin the optimization, the initial value of height  $h_0$  is determined based on a criterion comparing structural strength and stiffness. Specifically, it equals  $h_{str}$  for the case where  $Q$  is larger than  $[Q]$  and  $h_{stf}$  for  $Q$  less than  $[Q]$  (Wang & Yu, 2017).

$$h_{str} = \sqrt{\frac{QIK}{4\delta[\sigma]\left(\frac{2}{3} + \alpha\right)}}, h_{stf} = \sqrt[3]{\frac{Q^2l[\beta]C_2}{24E\delta\left(\frac{2}{3} + \alpha\right)}}, [Q] = \left(\frac{A_1}{1 + B_1}\right)^3 \tag{1}$$

where parameters  $K, A_1$  and  $B_1$  are

$$K = \left[ \frac{A_2}{2} + \sqrt{\left(\frac{A_2}{2}\right)^2 + B_2} \right]^2, \\ A_1 = \frac{[\sigma]}{\left(\varphi_2 + \varphi_1 \frac{P_t}{Q}\right) C_1} \left[ \left(\frac{C_2[\beta]}{3E}\right)^2 \left(\frac{2}{3} + \alpha\right) \delta l \right]^{\frac{1}{3}}, \\ B_1 = \frac{\varphi_1 l^{\frac{5}{3}} \rho_c (1 + \lambda)}{\left(\varphi_2 + \varphi_1 \frac{P_t}{Q}\right) C_1} \left[ \frac{C_2[\beta]}{3EQ^2} \left[\delta\left(\frac{2}{3} + \alpha\right)\right]^2 \right]^{\frac{1}{3}},$$

where parameters  $A_2$  and  $B_2$  in  $K$  are

$$A_2 = \varphi_1 l^{\frac{3}{2}} \rho_c (1 + \lambda) \sqrt{\frac{\delta}{[\sigma]Q} \left(\frac{2}{3} + \alpha\right)}, B_2 = \left(\varphi_2 + \varphi_1 \frac{P_t}{Q}\right) C_1.$$

where  $C_1 = (1 - l_1/2l)^2$  and  $C_2 = (1 + P_t/Q)(1 - l_1/l)[3 - (1 - l_1/l)^2]/2$  (Zhang et al., 2013).

Furthermore, initial values for thickness  $\delta_3$  takes 1.5 times  $\delta_1$ , and the width  $b$  does 0.4 times  $h_0$ .

### 2.3 Dependant Variables

Dependant variables refer to the dimensions of five types of stiffeners, such as ribs on web and flange, full diaphragms with hole, stiffeners around diaphragm hole, short diaphragms, trapezoid stiffeners, as shown in Fig. 2d. Parameters, such as numbers, locations and dimensions of all stiffeners are concerned (see Fig. 2e), and their relations with girder section follow the principle of local stability and manufacturing requirements. Accordingly, the number  $n_{rw}$ , location  $h_i$  of web ribs and distance  $d$  between adjacent diaphragms follow

$$\begin{aligned} \text{a. If } \frac{h_0}{\min(\delta_1, \delta_2)} &\leq 160 \sqrt{\frac{235}{\sigma_s}}, n_{rw} = 0, d = 2h_0, \\ \text{b. If } \frac{h_0}{\min(\delta_1, \delta_2)} &\leq 240 \sqrt{\frac{235}{\sigma_s}}, n_{rw} = 1, h_1 = 0.2h_0, d = 2(h_0 - h_1), \\ \text{c. If } \frac{h_0}{\min(\delta_1, \delta_2)} &\leq 320 \sqrt{\frac{235}{\sigma_s}}, n_{rw} = 2, h_1 = 0.2h_0, h_2 = 0.4h_0, d = 2(h_0 - h_2), \\ \text{d. If } \frac{h_0}{\min(\delta_1, \delta_2)} &> 320 \sqrt{\frac{235}{\sigma_s}}, n_{rw} = 3, h_1 = 0.2h_0, h_2 = 0.35h_0, h_3 = 0.5h_0, d = 2(h_0 - h_3), \end{aligned} \tag{2}$$

where ‘ $\min(\delta_1, \delta_2)$ ’ denotes the smaller one of  $\delta_1$  and  $\delta_2$ .  $\sigma_s$  denotes the yielding stress taking 235 MPa for Q235 structural steel. Noteworthy, the final distance  $d$  mandates to take 2 m when  $d$  is larger than 2 m. The width  $b_{rw}$  of rectangular-section rib takes

$$\begin{aligned} \text{a. If } d/h_0 \leq 0.85, b_{rw} &= \max(\delta_1, \delta_2) \left( \frac{4.5h_0}{\delta_{rw}} \right)^{1/3}, \\ \text{b. If } d/h_0 > 0.85, b_{rw} &= \max(\delta_1, \delta_2) \left[ 3 \left( 2.5 - \frac{0.45d}{h_0} \right) \left( \frac{d}{h_0} \right)^2 \frac{h_0}{\delta_{rw}} \right]^{1/3} \end{aligned} \quad (3)$$

where ‘ $\max(\delta_1, \delta_2)$ ’ denotes the larger one of  $\delta_1$  and  $\delta_2$ .

For flange ribs with rectangular section, the number  $n_{rf}$  follows,

$$\begin{aligned} \text{a. If } \frac{b}{\delta_3} \leq 60 \sqrt{\frac{235}{\sigma_s}}, n_{rf} &= 0, \\ \text{b. If } \frac{b}{\delta_3} \leq 120 \sqrt{\frac{235}{\sigma_s}}, n_{rf} &= 1, \\ \text{c. If } \frac{b}{\delta_3} > 120 \sqrt{\frac{235}{\sigma_s}}, n_{rf} &= 2. \end{aligned} \quad (4)$$

The width  $b_{rf}$  takes

$$b_{rf} = \delta_3 \left[ \frac{3n_{rf}d^2}{b\delta_{rf}} \left( 0.64 + \frac{0.09d}{b} \right) \right]^{1/3}. \quad (5)$$

For full diaphragms, the number  $n_d$  follows

$$\begin{aligned} \text{a. If } l/d \text{ is even, } n_d &= l/d - 1. \\ \text{b. If } l/d \text{ is not even, } n_d &\text{ takes the largest even number less than } l/d + 1. \end{aligned} \quad (6)$$

The width  $b_w$  ( $b_f$ ) takes  $1.2(h_0/30 + 0.04)$  with the unit of meter (m), and the thickness  $\delta_d$  takes  $\frac{b_w}{15} \sqrt{\frac{\sigma_s}{235}}$  to keep the shear stability of diaphragm. Noteworthy, in later APDL optimization process, widths  $b_w$  ( $b_f$ ) may takes the values approaching to  $b_{rw}$  ( $b_{rf}$ ), leading to an error due to boolean calculation accuracy when meshing finite element model. To deal with it, equations  $b_w$  ( $b_{rw}$ ) =  $\max(b_w, b_{rw})$  and  $b_f$  ( $b_{rf}$ ) =  $\max(b_f, b_{rf})$  are additionally defined.

For stiffeners around diaphragm hole, the width  $b_h$  and thickness  $\delta_h$  follow

$$b_h = \frac{\max(h_0 - 2b_f, b - 2b_w)}{17} \sqrt{\frac{\sigma_s}{235}}, \delta_h = b_h/13 \quad (7)$$

Besides, an arc-shaped fillet is designed to mitigate stress concentration at corner between adjacent stiffeners, the radius of which  $R_f$  follows

$$\begin{aligned} \text{a. If } \min(h_0 - 2b_f, b - 2b_w) > 0.6, R_f &= 0.3\text{m}, \\ \text{b. If } \min(h_0 - 2b_f, b - 2b_w) > 0.5, R_f &= 0.25\text{m}, \\ \text{c. If } \min(h_0 - 2b_f, b - 2b_w) > 0.4, R_f &= 0.2\text{m}, \\ \text{d. If } \min(h_0 - 2b_f, b - 2b_w) < 0.4, R_f &= 0. \end{aligned} \quad (8)$$

For short diaphragms, the height  $h_{sd}$  follows Eq. (9), and the locations  $h_1$  and  $h_2$  for web ribs originally defined in Eq. (2) are refreshed.

$$\begin{aligned} \text{a. If } n_{rw} = 0, h_{sd} &= 0.3h_0. \\ \text{b. If } n_{rw} = 1, h_{sd} &= b_f + R_f, h_1 = h_{sd}. \\ \text{c. If } n_{rw} = 2, h_{sd} &= h_2, h_1 = b_f + R_f. \\ \text{d. If } n_{rw} = 3, h_{sd} &= h_3, h_1 = b_f + R_f, h_2 = (h_1 + h_3)/2. \end{aligned} \quad (9)$$

Additionally, the number  $n_{sd}$  of short diaphragms between adjacent full diaphragms follows:

$$\begin{aligned} \text{a. If } d/0.6 < [d/0.6], n_{sd} &= [d/0.6] - 1, \\ \text{b. If } d/0.6 > [d/0.6], n_{sd} &= [d/0.6], \end{aligned} \quad (10)$$

where ‘ $[x]$ ’ denotes the nearest integer to  $x$ . By defining Eq. (10), the distance between adjacent short diaphragms will be less than 0.6m, which is the allowable maximum as per manual (Wan et al., 2008; Wang et al., 2013).

Further, trapezoid stiffeners are required at the edge of top flange to support the railway for trolley running. Considering the local stability, the length of upper side  $b_c$  takes the cantilever part of top flange, where  $b_c = 10\delta_3 \sqrt{235/\sigma_s}$ .

To reduce the number of design variables, the left side  $h_c$  takes  $b_f$ . Two opposite shorter sides take half the length  $b_c$  or  $h_c$ . The thickness, number and location follow the short diaphragms.

In optimization process, the thickness of web, flange and all stiffeners keep even and greater than 6 mm. Additionally, the length and width take the unit of meter, with the accuracy to centimeter.

## 2.4 Constraints on State Variables

State variables refer to the mechanical property of crane girder structure under specified load cases, such as the stress, deformation and frequency, which are regarded as the function of design variables. In optimization process, constraints on state variables provides the boundary for design variables changing. Further, to gain the lightest mass for crane girder structure, four possible optimization models (OM1, OM2,

OM3, OM4) are constructed in this paper in terms of the constraints on state variables.

For OM1, the strength and stiffness of crane girder in vertical impact (VI) case needs considered. Specifically, for strength, the maximum normal stress in mid-span  $\sigma_1$ , shear stress at the ends  $\tau_1$ , and von mises stress  $\sigma_{e1}$  are captured where coefficient  $\varphi_1$  are added on crane girder mass  $P_c$  (distribution load applied by gravity acceleration  $g$ ) and trolley mass  $P_t$  (concentrated load), and  $\varphi_2$  on goods weight  $Q$  (concentrated load). For stiffness, the static vertical deformation in mid span  $d_1$  is also involved, where the mass  $P_t$  and weight  $Q$  are without  $\varphi_1$  or  $\varphi_2$ . Correspondingly, constraints on state variables in OM1 are  $0 \leq \sigma_1 \leq [\sigma]$ ,  $0 \leq \tau_1 \leq [\tau]$ ,  $0 \leq \sigma_{e1} \leq [\sigma]$  and  $0 \leq d_1 \leq l/[\beta]$ , where  $[\sigma]$  takes  $\sigma_s/1.48$  and  $[\tau]$  does  $[\sigma]/1.73$ .

For OM2, besides the constraints in OM1, those on stresses and deformations in transverse impact case (TI) are captured and issued by  $0 \leq \sigma_2 \leq [\sigma]$ ,  $0 \leq \tau_2 \leq [\tau]$ ,  $0 \leq \sigma_{e2} \leq [\sigma]$  and  $0 \leq d_2 \leq l/[\beta_1]$ , where coefficient  $\varphi_5$  is added on mass  $P_c$  (distributed load with  $a$ ),  $P_t$  (concentrated load with  $a/g$ ) and weight  $Q$  (concentrated load with  $a/g$ ) in transverse direction besides those in vertical direction without  $\varphi_5$ .

For OM3, besides the constraints in OM1, the vertical frequency  $f$  of crane girder in dynamic vibration case (DV) is captured additionally, the constraint on which is  $f \geq [f]$ , where  $[f]$  is the lower limit of allowable frequency,  $[f] = 2$  Hz.

For OM4, all mentioned state variables, the normal stress, shear stress, von mises stress and deformations in VI and TI cases, the frequency in DV case, needs constrained as mentioned.

Further, to calculate all mentioned state variables, ANSYS parameter design language (APDL) programs are coded where SHELL63 element is employed to mesh grid. Convergence test shows that a total of 15,881 elements is adequate to obtain the structural stress, deformation and frequency, as shown in Fig. 2f. For boundary condition, element grid nodes on bottom flange of four end plates are constrained in  $x$ ,  $y$  or  $z$ - axial displacements (UX, UY, UZ) to form hinge supports as a whole. For load, concentrated loads, such as trolley mass  $P_t$  and weight  $Q$ , are applied to crane girder via wheel load  $P_w$  where  $P_w = (\varphi_1 P_t + \varphi_2 Q)/4$  for VI case. Further, to mitigate the effect of stress concentration,  $P_w$  is divided into  $n$  equal sub-loads  $P_n$  ( $P_n = P_w/n$ ), acting on the nodes in the area measured by  $l_w \times \delta_1$  at junction of web and flange, as illustrated in Fig. 2g, where  $l_w = 3.25(I_n/\delta_1)^{1/3}$  and  $I_n = I_r + I_f$ .  $I_f$  and  $I_r$  denote the inertia moments of the flange and trolley railway. Specifically,  $I_r$  takes  $1530.12 \text{ cm}^4$  for  $P_f \leq 340 \text{ MPa}$ ,  $2806.11 \text{ cm}^4$  for  $340 \text{ MPa} < P_f \leq 394 \text{ MPa}$ , and  $4796.71 \text{ cm}^4$  for  $P_f > 394 \text{ MPa}$ , where  $P_f$  is the fatigue load of wheels and  $P_f = (3\varphi_1 P_t + 2\varphi_2 Q)/12$  (Wang & Yu, 2017).

## 2.5 Optimization Method

With the objective of minimizing the mass of the crane girder, we employ a sequential approach involving Sub-Problem Approximation (SPA), Sweep (SW), and First-Order (FO) methods. In this sequence, SW takes the optimal result from SPA as the initial value, and FO considers both the optimal results from SPA and SW as the initial values.

In APDL, the SPA, SW and FO methods are conducted by coding ‘OPTYPE SUBP’, ‘OPTYPE SWEEP’ and ‘OPTYPE FIRST’, respectively. In terms of parameter settings, for SPA, the maximum iteration is set to 50, and the maximum number of consecutive infeasible design sets is limited to 5, where the expression ‘OPSUBP, 50, 5’ is coded. In SW, each design variable undergoes 10 divisions, where the expression ‘OPSWEEP, BEST, 10’ is coded. Regarding FO, the maximum iteration count is set at 50. However, further verification is needed to determine suitable values for the searching step ( $L_f$ ) and forward difference step ( $F_f$ ), where the expression ‘OPFIRST, 50,  $L_f$ ,  $F_f$ ’ is coded.

Additionally, the values of design variables need to be rounded up (RU) due to practical manufacturing requirements for two positions: sweep optimization finishing and convergence after FO, as illustrated in Fig. 1.

Ultimately, termination of the optimization process will be triggered when the gap between two adjacent masses achieves the specified tolerance (e.g., 0.01 times the mass in the current step), or when the maximum iteration or the maximum number of consecutive infeasible sets is reached.

Next, the variations of total crane mass (objective), dimensions of box section, ribs and diaphragms (design and dependant variables), as well as structural stresses, deformation and frequency (state variables), are analyzed in detail for four optimization models (OM1 ~ OM4) for each iteration.

## 3 Optimization Result

In this section, the optimization process and results of girder mass, dimensions of cross-section, diaphragm, and ribs are examined for three optimization methods (SPA, SW, and FO) across four optimization models (OMs), where SPA and SW are analyzed together.

### 3.1 SPA + SW Methods

#### 3.1.1 Crane Girder Mass

Figure 3a depicts a repetitive up-and-down cycle for iterations less than 10 across all OMs. Subsequently, it gradually diminishes its amplitude and endeavors to converge from the 10th to the 25th iteration in SPA, as illustrated in

**Fig. 3** Optimization of crane mass, girder section, ribs, diaphragms for SPA and SW

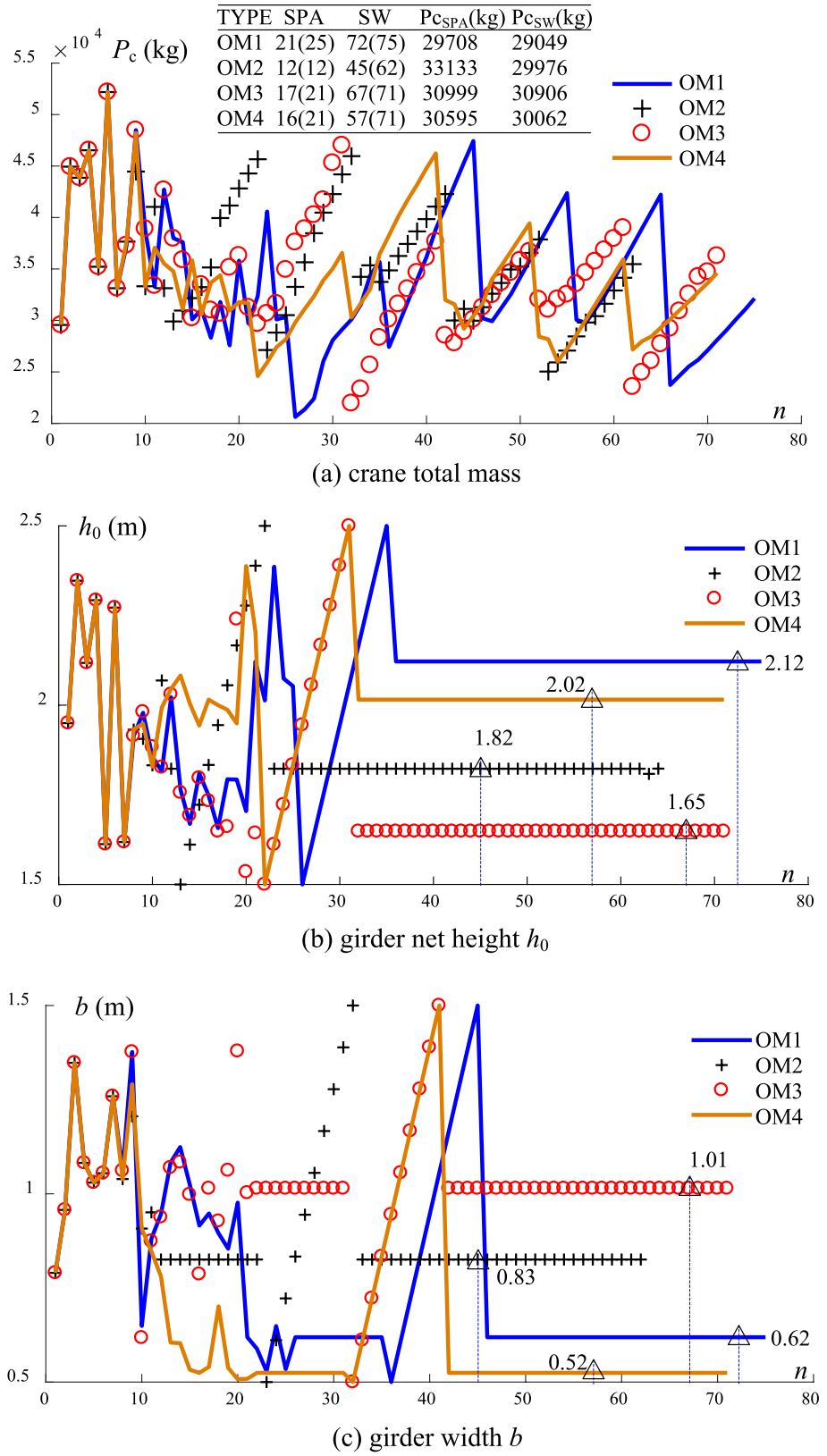


Fig. 3 (continued)

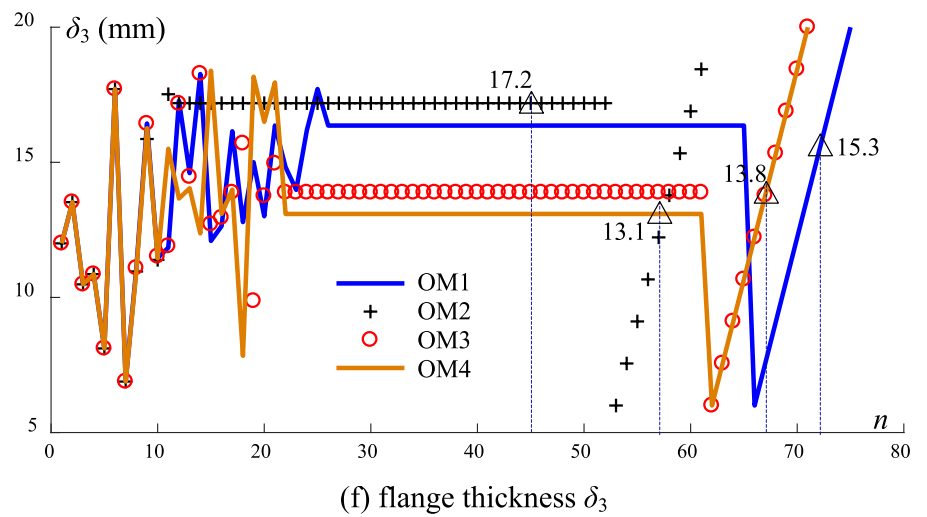
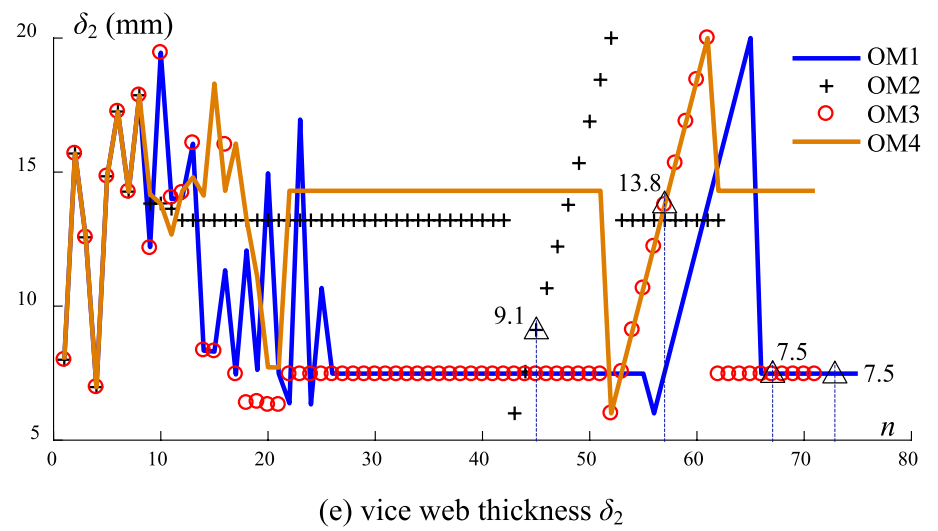
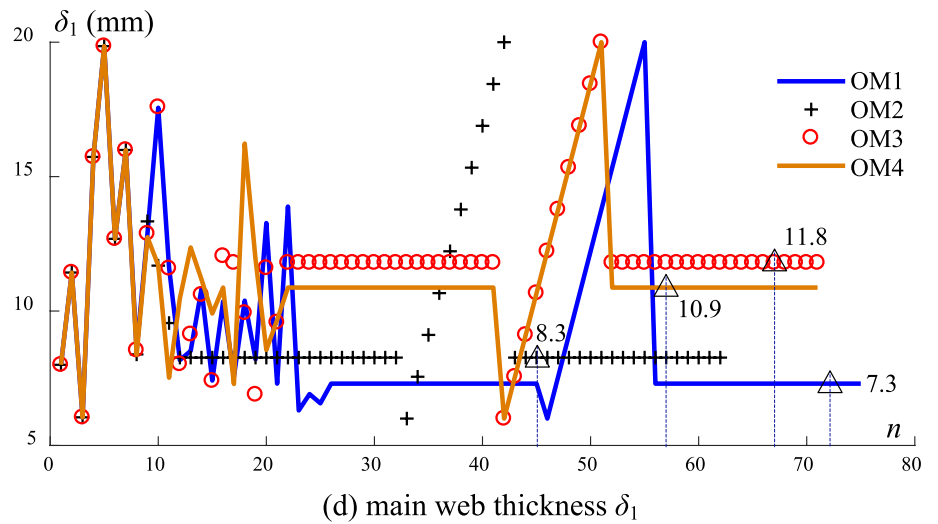
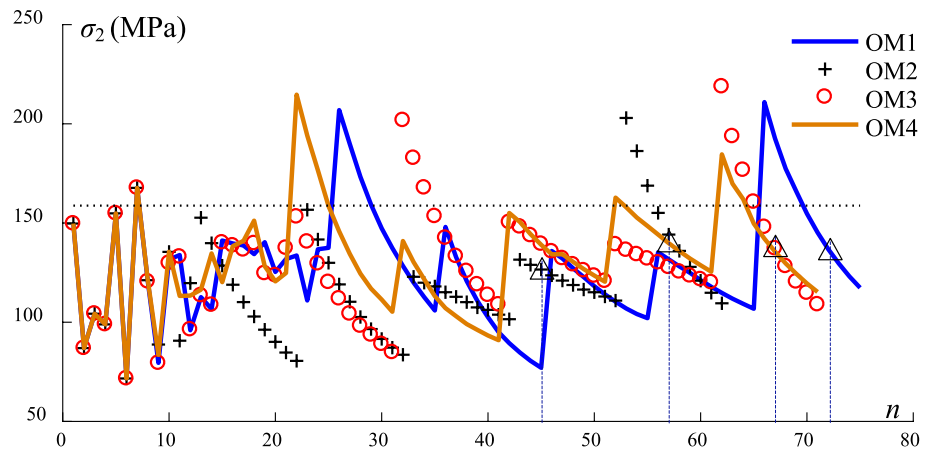
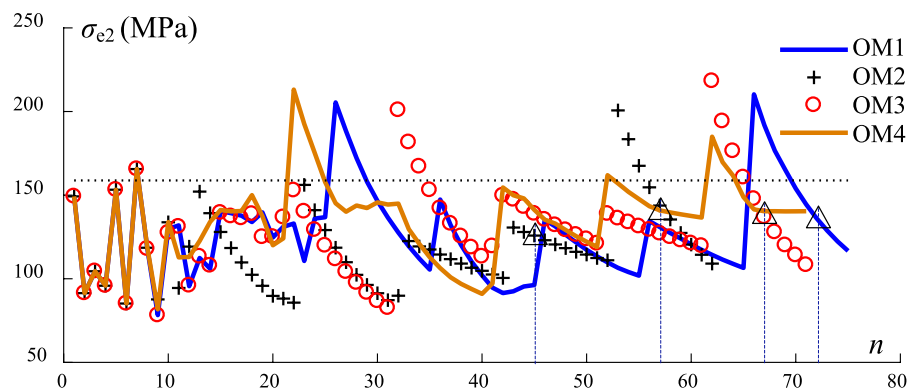




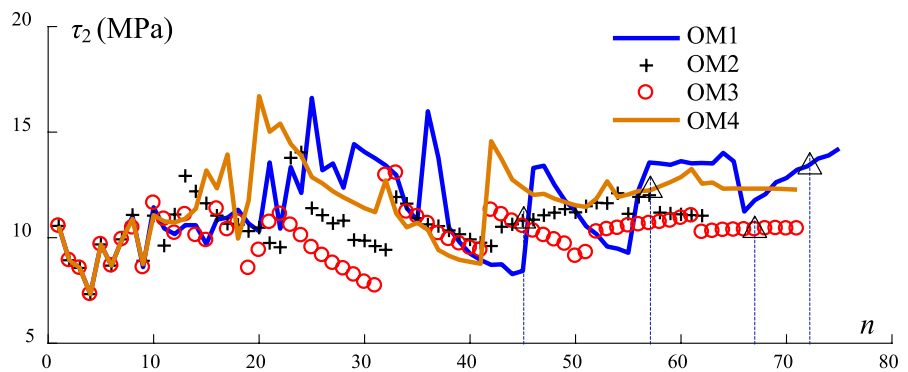
Fig. 3 (continued)



(g) normal stress in TI case  $\sigma_2$



(h) von-mises stress in TI case  $\sigma_{e2}$



(i) shear stress in TI case  $\tau_2$

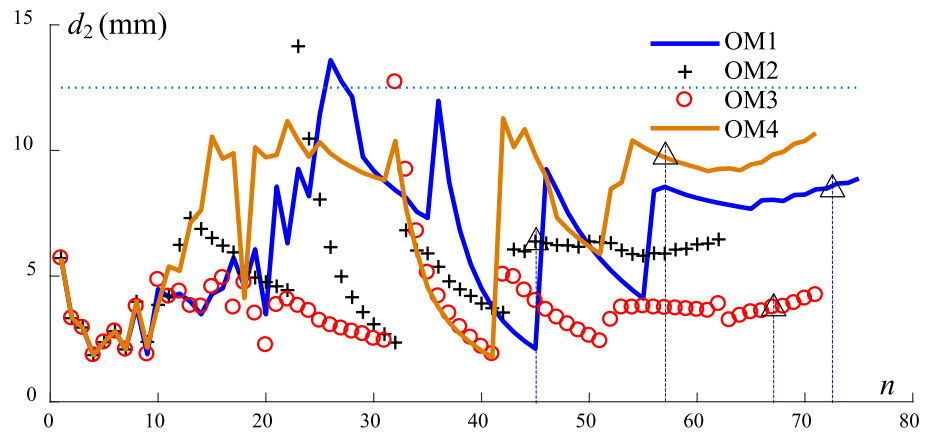
the corresponding table in Fig. 3a. Upon entering the SW period, 50 iterations proceed in a linearly increasing form from one design variable to another. The results reveal that the optimal mass for OM1 during the SPA period is 29,708 kg at the 21st iteration, decreasing further to 29,049 kg by the 72nd iteration in SW. Similarly, for OM2, the crane mass concludes at 33,133 kg in SPA and subsequently reduces to 29,976 kg in SW. For OM3, only a 93 kg weight gap is optimized from SPA to SW. Conversely, for OM4, the optimized

mass is 30,062 kg. By comparison, OM1 achieves the minimum mass after undergoing both SPA and SW periods.

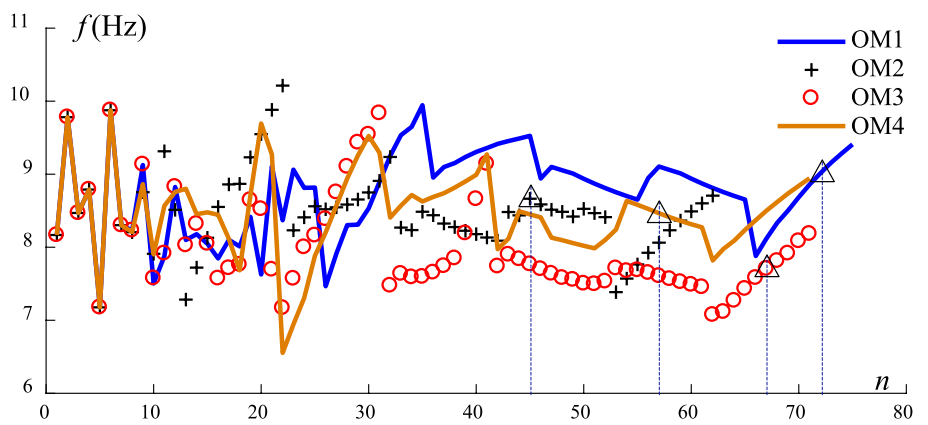
### 3.1.2 Dimensions of Girder Cross Section

In comparison to OM1, the optimized height  $h_0$  in SW for OM2 decreases from 2.12 m to 1.82 m (Fig. 3b), while the width  $b$  increases from 0.62 m to 0.83 m (Fig. 3c) due to the influence of stress and deformation from TI load case.

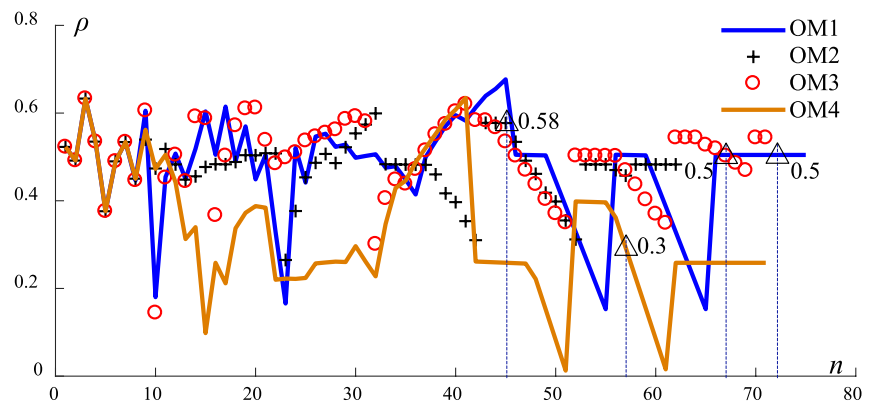
Fig. 3 (continued)



(j) transverse deformation in TI case  $d_2$



(k) vertical frequency in DV case  $f$



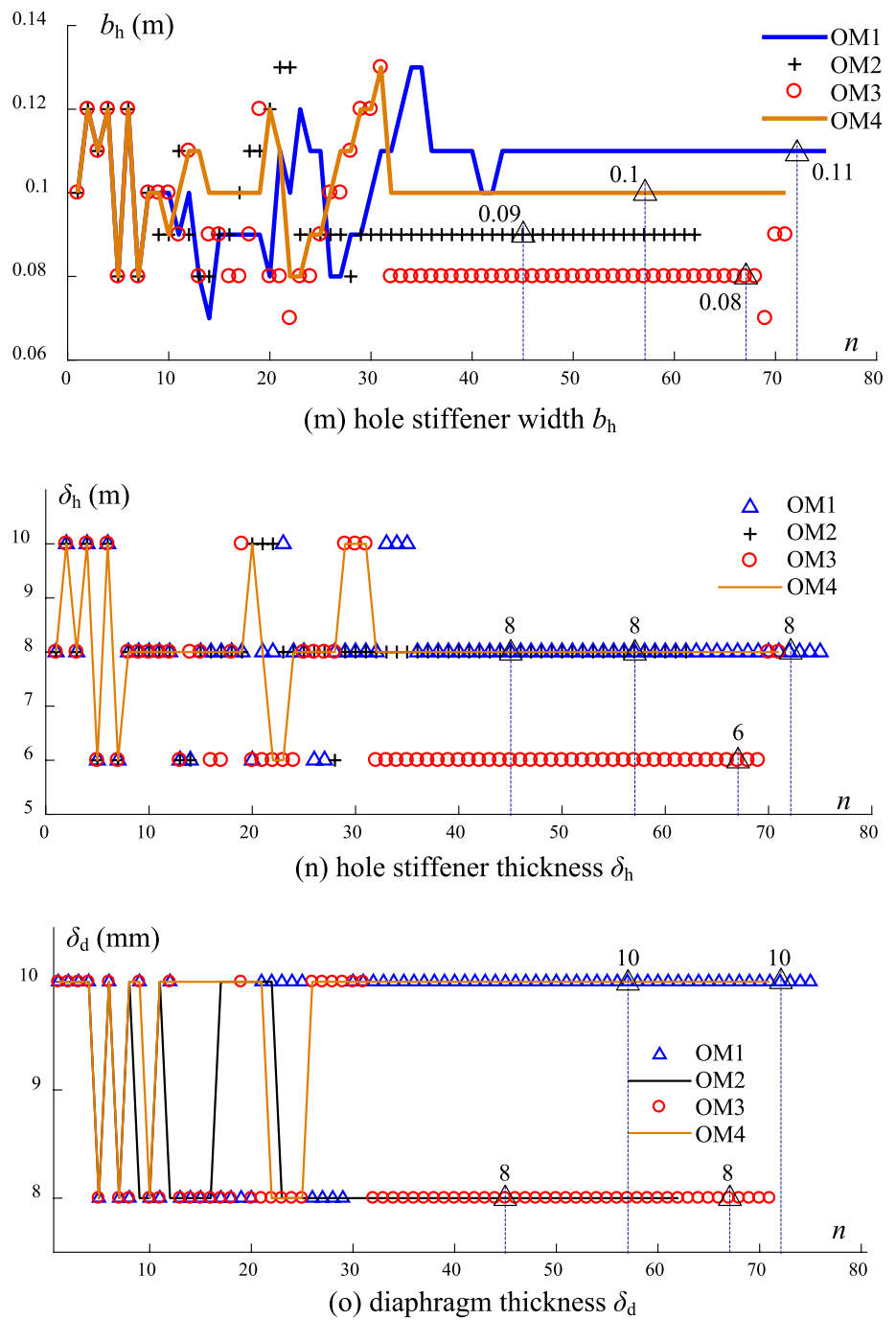
(l) area ratio of hole to diaphragm  $\rho$

Moreover, under the constraint on frequency in the DV case, the height  $h_0$  in OM3 further reduces to 1.65 m, while the width  $b$  increases to 1.01 m. For OM4, considering all load cases, both the height  $h_0$  and width  $b$  reduce to 2.02 m and 0.52 m, respectively, compared to OM1. Thus, incorporating constraints on TI and DV cases alongside VI significantly reduces both the height and width of girder section.

Conversely, introducing single additional constraints on TI or DV cases may lead to different opposite optimization directions between height and width.

Regarding plate thickness, for webs in Fig. 3d, e, the optimized thickness of the vice web approaches that of the main web for OM1. However, for OM3, the vice web is noticeably thinner than the main web, whereas for both OM2 and

Fig. 3 (continued)

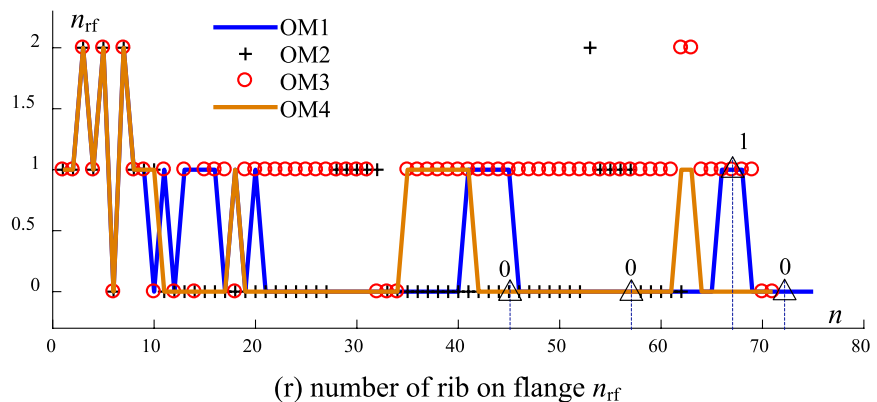
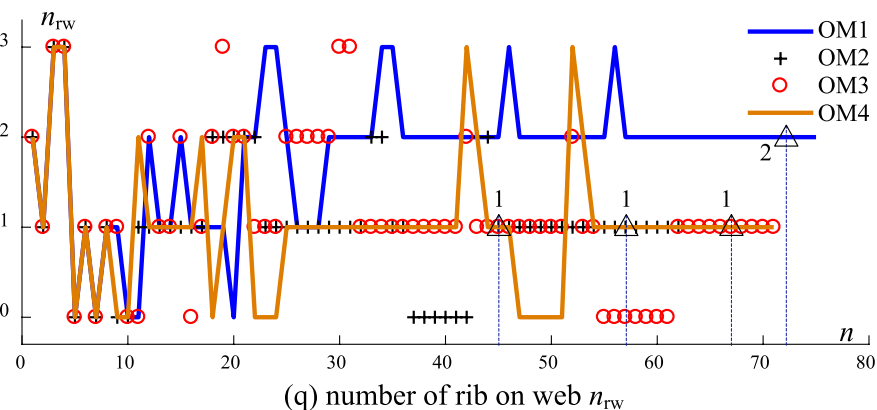
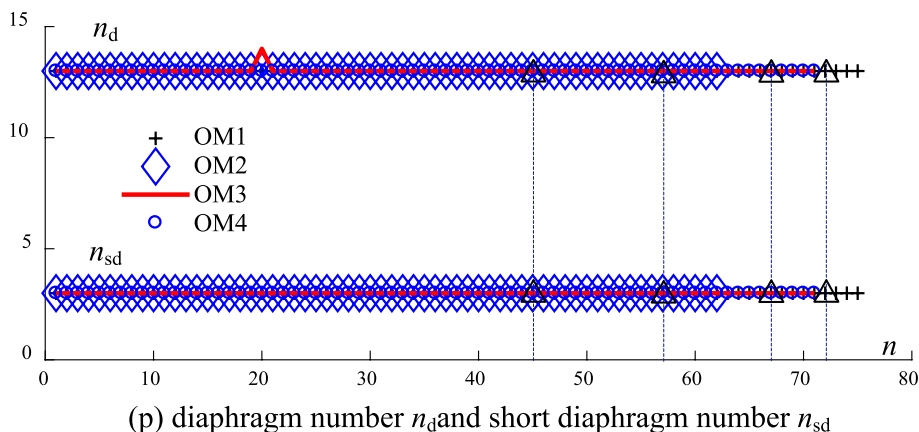


OM4, it is thicker. For flanges in Fig. 3f, the flange thickness is almost twice that of the web for both OM1 and OM2. In contrast, in OM4, the flange thickness (13.1 mm) is less than that of the vice web (13.8 mm). Overall, additional constraints on stress and deformations in the TI case or the frequency in the DV case lead to diverse optimization paths and results.

### 3.1.3 State Variables

In Fig. 3g–k, stresses and deformations in the TI case, as well as the frequency in DV for four OMs, are depicted. The dotted line represents the allowable limit. Notably, after conducting SPA and SW optimization, the optimized normal stress  $\sigma_2$  and von mises stress  $\sigma_{e2}$  in the TI case for all OMs are consistently below  $[\sigma]$  ( $[\sigma]=158$  MPa) and shear stress  $\tau_2$  is below  $[\tau]$  ( $[\tau]/1.73$ ). Moreover, the optimized transverse deformation  $d_2$  in TI is within the limit of 12.5 mm

Fig. 3 (continued)



( $l/2000$ ), and the frequency  $f$  in DV consistently exceeds 2 Hz, regardless of the OM type. This implies that, for a two-girder crane with a 25 m span and 100 t capacity, although there are no consideration on the constraints to the stresses, deformations, or frequency in TI or DV cases in OM1, OM2, or OM3, they do not exceed the allowable limit after SPA and SW optimization.

### 3.1.4 Diaphragms and Hole Stiffeners

The study focuses on the area ratio of the hole to the diaphragm to validate the appropriateness of setting a hole in

the diaphragm. The optimized ratios are 0.5, 0.58, 0.5, and 0.3 successively for four OMs, as depicted in Fig. 3l. Clearly, OM4 features the smallest hole, potentially requiring feasibility checks for manufacturing and routine maintenance accessibility. Consequently, a solid diaphragm without any holes may be preferred, provided the hole size is sufficiently small.

Regarding the stiffeners around the hole, OM3 exhibits the minimum width of 80 mm (Fig. 3m) and thickness of 6mm (Fig. 3n). This suggests that the diaphragm in OM3 is robust enough to maintain in-plane shear stability, thus reducing the need for additional stiffeners around the hole.

Furthermore, the variation of diaphragm thickness is depicted in Fig. 3o, where the optimized thickness of 8mm for both OM2 and OM3 is needed for diaphragm to ensure in-plane shear stability, compared to 10 mm for OM1 and OM4. This implies that the widths  $b_f$  and  $b_w$  on the diaphragm in OM1 and OM4 are correspondingly larger than those in OM2 and OM3, potentially resulting in a smaller hole in the diaphragm.

In addition, Fig. 3p reveals a consistent count of 13 diaphragms for all OMs, with a distance ( $d$ ) of 2 m between adjacent diaphragms. However, during the 20th iteration in OM3, the number unexpectedly increases to 14, and the distance  $d$  reduces to 1.84 m, falling below the upper limit of 2 m, due to the consideration of local buckling. In cases of 13 diaphragms, the number of short diaphragms between adjacent full ones remains at 3.

### 3.1.5 Ribs on Webs and Flanges

Two ribs are essential on the web in OM1, distinguishing it from other optimization models (OMs) that necessitate only one rib. This discrepancy underscores the larger ratio of height to thickness in the girder cross-section of OM1, mandating additional ribs for the maintenance of local web stability. Consequently, the short diaphragm height in OM1 is designed at 0.85 m, a notable deviation from other OMs. Similarly, in OM3, a singular rib is indispensable to support the flange, due to its substantial ratio of flange width

to thickness. This is in contrast to other OMs where such additional structural support is unnecessary, as elucidated in Fig. 3q, r.

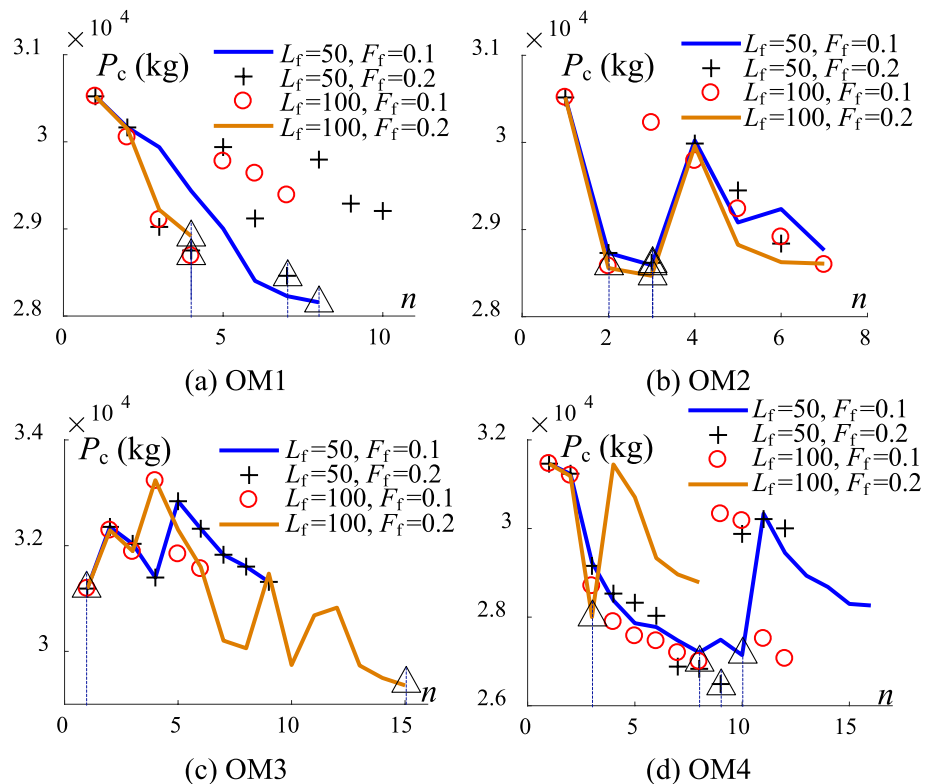
## 3.2 FO Method

In this section, the first-order method (FO) is employed to identify potential reductions in mass around the results obtained from SPA and SW. Initially, the mass result from SPA and SW is rounded up, and further optimization is conducted by FO under different combinations of the searching step ( $L_f$ ) and forward difference step ( $F_f$ ) for all OMs, as illustrated in Fig. 4. Specifically, optimization paths and results for different  $L_f$  and  $F_f$  are analyzed in the following.

### 3.2.1 Optimization Path

OM1 exhibits a consistent reduction in the case of ‘ $L_f=50$  and  $F_f=0.1$ ’ and ‘ $L_f=100$  and  $F_f=0.2$ ’, while others show an up-and-down cycle. For OM2, all curves decline significantly at the beginning and reach their minimum mass at the bottom around the 2nd or 3rd iteration. In contrast, the curves in OM3 initially rise and then converge after up-and-down cycles. Meanwhile, for OM4, with the convergence tolerance set at 200 kg, the minimum mass is reached at the 9th iteration, except for the case of ‘ $L_f=100$  and  $F_f=0.2$ ’, where the minimum mass is achieved at the 3rd iteration.

Fig. 4 FO optimization of crane mass in terms of  $L_f$  and  $F_f$



### 3.2.2 Optimization Results

There are three types in total for the occurrence of optimization results. Firstly, the optimized minimum mass occurs at the final convergence, as seen in the cases of ‘ $L_f=50$  and  $F_f=0.1$ ’ and ‘ $L_f=100$  and  $F_f=0.2$ ’ in OM1, and ‘ $L_f=100$  and  $F_f=0.2$ ’ in OM3. Secondly, the optimized mass occurs initially, including the cases of ‘ $L_f=50$ ’ and ‘ $L_f=100$  and  $F_f=0.1$ ’ in OM3, indicating that the FO method is redundant after SW in OM3. Thirdly, except for the aforementioned cases, the optimized mass occurs at the initial valley bottom before the final convergence.

### 3.3 Rounded-Up

To confirm the appropriate parameters  $L_f$  and  $F_f$  of FO method corresponding to the minimum crane mass, the FO results are once again rounded up and summarized in Tables 1 and 2 for all OMs.

#### 3.3.1 State Variables

The results indicate that, for the two-girder crane with a 25 m span and 100 t loading capacity, the stresses and deformations in the TI case and the frequency in DV are

**Table 1** Rounded-up dimensions, mass, stresses, deformation and frequency of crane structure based on FO optimization results for OM1 and OM2

TYPE	OM1				OM2			
	$L_f=50$	$L_f=50$	$L_f=100$	$L_f=100$	$L_f=50$	$L_f=50$	$L_f=100$	$L_f=100$
$L_f$	50	50	100	100	50	50	100	100
$F_f$	0.1	0.2	0.1	0.2	0.1	0.2	0.1	0.2
Location	8th	7th	4th	4th	3rd	3rd	2nd	3rd
$h_0$ (mm)	2160	2160	2170	2120	1810	1810	1800	1800
$b$ (mm)	590	550	600	600	780	790	780	780
$b/h_0$	0.27	0.25	0.28	0.28	0.43	0.44	0.43	0.43
$\delta_1$ (mm)	8	8	8	8	8	8	8	8
$\delta_2$ (mm)	8	8	8	8	10	10	10	10
$\delta_3$ (mm)	16	18	16	16	18	18	18	18
$\delta_3/\min(\delta_1, \delta_2)$	2	2.25	2	2	2.25	2.25	2.25	2.25
$\delta_h$ (mm)	8	8	8	8	8	8	8	8
$\delta_d$ (mm)	10	10	10	10	8	8	8	8
$b_f$ (mm)	130	130	130	130	120	120	120	120
$b_w$ (mm)	130	130	130	130	130	130	130	130
$b_h$ (mm)	110	110	110	110	90	90	90	90
$b_c$ (mm)	160	180	180	180	180	180	180	180
$n_d$	13	13	13	13	13	13	13	13
$n_{sd}$	3	3	3	3	3	3	3	3
$n_{rw}$	2	2	2	2	1	1	1	1
$n_{rf}$	0	0	0	0	0	0	0	0
$h_1$ (mm)	130	130	130	130	370	370	370	370
$h_2$ (mm)	864	864	868	848	-	-	-	-
$h_{sd}$ (mm)	864	864	868	848	370	370	370	370
$R_f$ (mm)	0	0	0	0	250	250	250	250
$P_g$ (t)	20.98	21.34	21.16	20.85	23.81	23.95	23.74	23.74
$P_c$ (t)	30.32	30.76	31.88	31.42	30.31	30.48	30.23	30.23
$\gamma(1-P_g/P_c)$	0.31	0.31	0.34	0.34	0.21	0.21	0.21	0.21
$\sigma_1$ (MPa)	148.84	144.66	137.39	141.7	145.50	143.96	146.03	146.03
$\tau_1$ (MPa)	10.36	11.8	11.11	11.31	10.72	10.72	10.79	10.79
$\sigma_{e1}$ (MPa)	147.85	143.72	136.44	140.71	144.31	143.23	145.29	145.29
$\omega_1$ (mm)	27.66	26.63	25.18	26.50	31.66	31.41	32.03	32.03
$\sigma_2$ (MPa)	131.34	127.93	121.31	125.04	127.27	126.30	128.13	128.13
$\tau_2$ (MPa)	13.60	15.01	14.03	14.21	11.06	10.48	11.10	11.10
$\sigma_{e2}$ (MPa)	130.54	127.18	120.53	124.23	126.63	125.66	127.48	127.48
$\omega_2$ (mm)	8.62	9.81	8.53	8.70	7.19	7.05	7.22	7.22
$f$ (Hz)	9.13	9.25	9.35	9.19	8.60	8.61	8.56	8.56

$P_g$ : the mass of girder without stiffeners

**Table 2** Rounded-up dimensions, mass, stresses, deformation and frequency of crane structure based on FO optimization results for OM3 and OM4

TYPE	OM3				OM4			
	50	50	100	100	50	50	100	100
$L_f$								
$F_f$	0.1	0.2	0.1	0.2	0.1	0.2	0.1	0.2
Location	1st	1st	1st	15th	10th	9th	8th	3rd
$h_0$ (mm)	1650	1650	1650	1900	2130	2140	2110	2120
$b$ (mm)	1010	1010	1010	870	550	550	560	540
$b/h_0$	0.61	0.61	0.61	0.46	0.26	0.26	0.27	0.25
$\delta_1$ (mm)	12	12	12	10	10	10	10	10
$\delta_2$ (mm)	8	8	8	6	10	10	10	12
$\delta_3$ (mm)	14	14	14	16	16	16	16	16
$\delta_3/\min(\delta_1, \delta_2)$	1.75	1.75	1.75	2.67	1.6	1.6	1.6	1.6
$\delta_h$ (mm)	6	6	6	8	8	8	8	8
$\delta_d$ (mm)	8	8	8	8	10	10	10	10
$b_f$ (mm)	160	160	160	120	130	130	130	130
$b_w$ (mm)	160	160	160	130	130	130	130	150
$b_h$ (mm)	80	80	80	100	110	110	110	110
$b_c$ (mm)	140	140	140	160	160	160	160	160
$n_d$	13	13	13	13	13	13	13	13
$n_{sd}$	3	3	3	3	3	3	3	3
$n_{rw}$	1	1	1	2	1	1	1	1
$n_{rf}$	1	1	1	0	0	0	0	0
$h_1$ (mm)	460	460	460	420	130	130	130	130
$h_2$ (mm)	–	–	–	760	–	–	–	–
$h_{sd}$ (mm)	460	460	460	760	130	130	130	130
$R_f$ (mm)	300	300	300	300	0	0	0	0
$P_g$ (t)	24.05	24.05	24.05	22.86	23.63	23.71	23.60	25.09
$P_c$ (t)	31.54	31.54	31.54	32.01	29.00	29.09	28.97	30.68
$\gamma(1-P_g/P_c)$	0.24	0.24	0.24	0.29	0.19	0.18	0.19	0.18
$\sigma_1$ (MPa)	155.29	155.29	155.29	140.44	144.27	143.27	145.21	140.68
$\tau_1$ (MPa)	10.42	10.42	10.42	9.56	10.19	9.79	9.79	10.31
$\sigma_{e1}$ (MPa)	154.77	154.77	154.77	139.43	143.27	142.29	144.13	139.88
$\omega_1$ (mm)	37.07	37.07	37.07	29.40	27.28	26.99	27.65	26.63
$\sigma_2$ (MPa)	134.85	134.85	134.85	122.50	127.39	126.58	128.23	124.56
$\tau_2$ (MPa)	10.38	10.38	10.38	9.82	12.29	11.26	11.15	11.69
$\sigma_{e2}$ (MPa)	134.47	134.47	134.47	121.71	146.44	147.05	140.92	147.07
$\omega_2$ (mm)	3.73	3.73	3.73	4.74	10.18	10.16	9.93	10.20
$f$ (Hz)	7.71	7.71	7.71	8.60	9.32	9.35	9.26	9.17

within the specified allowable limits regardless of OMs. This implies that the optimized results for crane mass and girder dimensions remain feasible, even when disregarding the constraints on stresses or deformations in the TI case or frequency in DV.

### 3.3.2 Design Variables, Dependent Variables, and Crane Mass

In OM1, the optimized girder section has a web height of 2.1 m, requiring two ribs to maintain the web stable. Additionally, due to the narrow flange with a  $b/h_0$  ratio averaging 27%, there is no need to introduce an arc-shaped fillet at

the junction of hole stiffeners on the diaphragm. The final rounded-up crane mass ranges from 30 to 32t, with the proportion of stiffeners and end beams ( $\gamma$ ) averaging 32.5%.

For OM2, the rounded-up mass after FO further reduces to 1.8 m, where a single rib is sufficient for web stability. The flange thickness remains uniform at 18 mm, and unexpectedly, the vice web is thicker than the main one. The rounded-up mass primarily focuses on 30.3 t, with  $\gamma$  being uniformly 21%.

When compared to OM1 and OM2, most cases in OM3 have a wider flange with one rib to maintain local stability, resulting in a 24% proportion for stiffener and end beams. However, in the case of ' $L_f=100$  and  $F_f=0.2$ ', two ribs are

required for the web, while none are needed for the flange, leading to a total mass of 32 t and uneconomical utilization of structural strength and stiffness.

Additionally, compared to OM1, the optimized girder section in OM4 has a similar web height but a larger thickness for both main and vice webs, requiring just one rib for the web. The crane mass after rounding up effectively reduces to around 29 t.

In summary, through a comparison of parameters on  $L_f$  and  $F_f$  for all OMs, the best optimization model is OM4, and the minimum crane mass is achieved at 28.97 t when  $L_f$  is set to 100 and  $F_f$  to 0.1.

### 4 Comparison with Four Intelligence Algorithms

To demonstrate the advantage of the proposed method (PM) in optimizing the girder structure, a comparison is made between the optimized results from PM and four intelligence algorithms (IAs)—Grey Wolf Optimizer (GWO), Whale Optimization Algorithm (WOA), Particle Swarm Optimization (PSO), and Genetic Algorithm (GA), respectively (Su et al., 2022). For analysis, a crane

with a 300t loading capacity and a 28.9 m span length is considered. The trolley mass is 173t, the distance between wheels is 3.15 m, the yielding stress is 355 MPa, and the allowable stress is 239.86 MPa. The upper limits for deformations in the vertical and transversal directions are calculated as 57.8 mm and 14.45 mm, respectively, with other parameters referring to the aforementioned 100t case.

Initial values and optimized results between PM and four IAs are compared in Table 3. Specifically, the optimized girders from four IAs have similar structural features. That is, for all four IAs, although the mass of one girder is optimized to around 40 t from 57.29 t, either the stresses or deformations unexpectedly exceed their allowable upper limits. Besides, the optimized section is almost square, and the thickness of the flange is uniformly smaller than those of the main web, which requires only one rib for the web while two for the flange to maintain local stability. Consequently, the optimized girder sections obtained from the four IAs prove unsuitable for scenarios where the moments induced by vertical loads outweigh those induced by transverse loads, which means these four IAs are irrational. Comparably, the optimized girder from PM has a much smaller ratio of width to height, requiring three ribs for the web and none for the flange, which has a much

**Table 3** Comparison of the initial values and optimization results between PM and IAs

Method	IAs (Su et al., 2022)					PM	
	Initial	GWO	WOA	PSO	GA	Initial	Optimized
$h_0$ (mm)	2960	2030	2035	2030	2030	2790	2880
$b$ (mm)	1978	2268	2463	1934	1871	1130	820
$b/h_0$	0.67	1.12	1.21	0.95	0.92	0.41	0.28
$\delta_1$ (mm)	14	18	18	20	20	10	16
$\delta_2$ (mm)	10	12	12	12	12	10	6
$\delta_3$ (mm)	20	16	16	18	18	16	22
$\delta_3/\min(\delta_1, \delta_2)$	2	1.33	1.33	1.5	1.5	1.6	3.67
$n_{rw}$	3	1	1	1	1	3	3
$n_{rf}$	2	2	2	2	2	1	0
$h_1$ (mm)	530	470	470	510	510	480	576
$h_2$ (mm)	1005	–	–	–	–	937.5	1000
$h_{sd}$ (mm)	1480	470	470	510	510	1395	1440
$R_f$ (mm)	300	300	300	300	300	300	0
$P_{c-one}$ (t)	57.29	40.48	42.75	40.49	39.80	34.84	35.69
$\sigma_1$ (MPa)	166.76	243.53	235.55	234.09	237.22	270.80	231.16
$\tau_1$ (MPa)	29.34	30.94	31.17	33.08	33.49	24.30	26.50
$\sigma_{e1}$ (MPa)	239.79	304.70	271.71	226.15	225.44	282.94	228.96
$\omega_1$ (mm)	27.10	60.47	57.49	59.74	60.93	53.11	46.06
$\sigma_2$ (MPa)	146.71	212.54	205.44	204.62	207.40	243.29	205.46
$\tau_2$ (MPa)	24.80	26.23	26.55	28.02	28.35	24.90	15.15
$\sigma_{e2}$ (MPa)	205.24	265.43	237.13	199.99	202.04	246.65	224.54
$\omega_2$ (mm)	3.46	2.93	2.81	3.75	3.95	10.52	13.51
$f$ (Hz)	8.72	9.09	9.54	8.14	7.96	7.92	8.26

$P_{c-one}$ : mass of one crane girder



stronger resistance to vertical loads compared to IAs. Correspondingly, the mass of the crane girder is effectively optimized to 35.69 t, and simultaneously all stresses and deformations are within the allowable limits. Obviously, compared to IAs, the utilization of both structural strength and stiffness in PM is notably enhanced under the condition of lighter structure and the serious limit on stress and deformation.

Besides the difference in algorithm theory, the reason behind the different optimized results between PM and four IAs lies in that PM takes the total mass of one girder as the objective while IAs take the area of the girder section. Correspondingly, the dimensions, numbers, and locations of diaphragms and ribs are real-time optimized following the girder section in PM, while those are not considered due to the sensitivity analysis and thus remain unchanged in IAs. This further means the influence of diaphragms and ribs on girder mass and stresses and deformations in each iteration for optimization is precisely considered in PM while not in IAs, which definitely leads to different optimization speeds and paths and thus different results.

### 5 Parameter Study

In this section, an overhead crane with a 25 m span and 100 t loading capacity is taken as an example to investigate the effects of stiffness coefficient and material property on the optimization process and rounded-up results based on the chosen 4th model considering constraints on stresses and deformations in VI and TI cases and frequency in DV, with  $L_f$  set to 100 and  $F_f$  to 0.1.

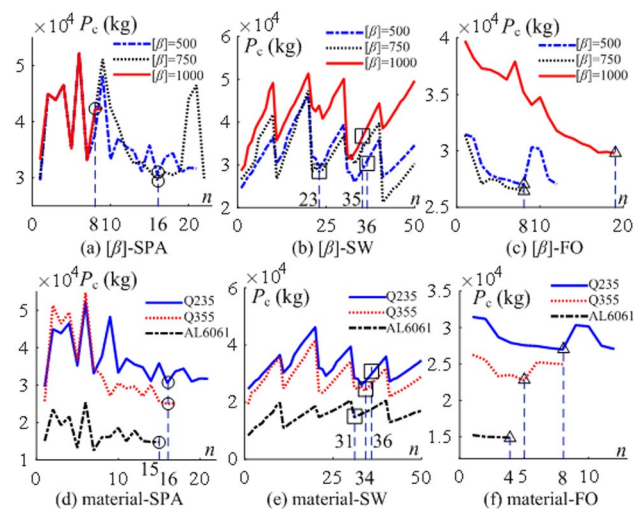


Fig. 5 Effect of stiffness coefficient and material on SPA, SW and FO processes

### 5.1 Optimization Process

#### 5.1.1 The Effect of Stiffness Coefficient

Cases of ‘ $[\beta] = 500$ ’, ‘ $[\beta] = 750$ ’, and ‘ $[\beta] = 1000$ ’ are respectively designated as the constraints on vertical deformation in VI case. Comparison in Fig. 5a shows that the case of ‘ $[\beta] = 1000$ ’ converges at the fastest speed compared to others, reaching the minimum mass of 42 t at the 8th iteration for the SPA period, while the cases of ‘ $[\beta] = 500$ ’ and ‘ $[\beta] = 750$ ’ however require 16 iterations to reach their optimum mass of 30 t. The reason for the gap in convergence speed between them lies in the strong constraint on structural deformation in the case of ‘ $[\beta] = 1000$ ’. Similarly, for the SW period in Fig. 5b, it is evident that the case of ‘ $[\beta] = 1000$ ’ still holds the largest. When it comes to the FO period in Fig. 5c, the mass for ‘ $[\beta] = 1000$ ’ drops significantly to 29.8 t at the 19th iteration, while the cases of ‘ $[\beta] = 500$ ’ and ‘ $[\beta] = 750$ ’ achieve their minimum mass of around 26 t at the 8th.

#### 5.1.2 The Effect of Material Property

Optimizations on overhead cranes made of Q235 steel, Q355 steel, and aluminum alloy 6061-T6 (Damian & Tomasz, 2016) (AL6061, with Young’s modulus of 68.9 GPa, density of 2700 kg/m<sup>3</sup>, Poisson’s ratio of 0.33, yielding stress of 276 MPa) are conducted. Results show that the value of crane mass for the AL6061 case constantly remains the least for SPA, SW, and FO. Specifically, in SPA (Fig. 5d), the optimized mass for the AL6061 case is 14.76 t, almost half that of Q235 steel, while the mass for Q355 steel is 24.95 t. In the SW period (Fig. 5e), all crane masses are optimized by a small quantity, with the results being 23.91 t for Q355 steel and 14.72 t for AL6061 due to the reduction of the thickness of the vice

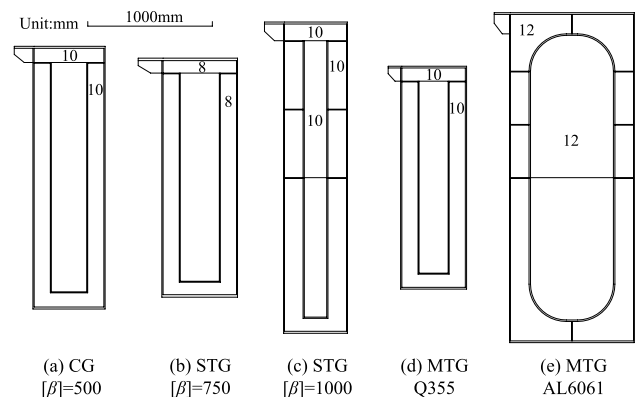


Fig. 6 Optimized configuration of cross section after rounded-up for two-girders crane with 25 m span and 100 ton loading capacity

**Table 4** Rounded-up dimensions, mass, stress, deformation and cost from FO results

Material	Q235	Q235	Q235	Q355	AL6061
$[\beta]$	500	750	1000	500	500
$h_0$ (mm)	2110	1920	2500	1790	2650
$b$ (mm)	560	590	500	510	990
$b/h_0$	0.27	0.31	0.20	0.28	0.37
$\delta_1$ (mm)	10	10	6	10	6
$\delta_2$ (mm)	10	8	6	10	6
$\delta_3$ (mm)	16	20	16	14	14
$\delta_3/\min(\delta_1, \delta_2)$	1.6	2.5	2.67	1.4	2.33
$\delta_h$ (mm)	8	8	10	8	12
$\delta_d$ (mm)	10	8	10	10	12
$b_f$ (mm)	130	120	150	120	170
$b_w$ (mm)	130	130	150	130	150
$b_h$ (mm)	110	100	130	110	150
$b_c$ (mm)	160	200	160	110	130
$n_d$	13	13	13	13	13
$n_{sd}$	3	3	3	3	3
$n_{rw}$	1	1	3	1	3
$n_{rf}$	0	0	0	0	1
$h_1$ (mm)	130	120	150	120	470
$h_2$ (mm)	–	–	700	–	897.5
$h_3$ (mm)	–	–	1250	–	1325
$h_{sd}$ (mm)	130	120	1250	120	1325
$R_f$ (mm)	0	0	0	0	300
$P_g$ (t)	23.60	22.83	18.06	19.66	8.04
$P_c$ (t)	28.97	28.26	30.18	24.03	14.98
$\gamma (1-P_g/P_c)$	0.19	0.19	0.40	0.18	0.46
$\sigma_1$ (MPa)	145.2(9%)	147.4(7%)	144.7(9%)	202.7(16%)	90.7(51%)
$\tau_1$ (MPa)	9.8(89%)	10.04(89%)	10.5(89%)	11.4(92%)	7.3(93%)
$\sigma_{e1}$ (MPa)	144.1(9%)	146.2(8%)	144.3(9%)	201.4(16%)	100.5(46%)
$\omega_1$ (mm)	27.7(45%)	29.8(11%)	24.0(4%)	45.9(8%)	47.7(5%)
$\sigma_2$ (MPa)	128.2(19%)	129.7(18%)	129.3(19%)	178.5(26%)	79.9(57%)
$\tau_2$ (MPa)	11.2(88%)	11.1(88%)	12.2(87%)	13.0(91%)	8.0(93%)
$\sigma_{e2}$ (MPa)	140.9(11%)	140.3(12%)	128.9(19%)	177.5(26%)	85.1(54%)
$\omega_2$ (mm)	9.9(21%)	10.7(14%)	11.7(7%)	11.5(8%)	11.9(5%)
$f$ (Hz)	9.3	9.1	9.8	7.9	9.9
Price (USD)	23,176	22,608	24,144	19,224	23,968

web at the 4th cycle. When it comes to the FO period (Fig. 5f), the crane mass for AL6061 optimizes at 14.88 t on convergence, while Q355 reaches 22.76 t at the 5th and Q235 does 27 t at the 8th.

### 5.2 Rounded-Up

Starting from the former FO results, dimensions of the girder cross-section and stiffeners are rounded up and displayed in Fig. 6 in terms of stiffness coefficient and material property, and the corresponding mass, mechanical performance, and total predicted cost are analyzed in Table 4 for detail.

#### 5.2.1 Dimensions

Compared to the case of Q235 steel with ‘ $[\beta] = 500$ ’, the case ‘ $[\beta] = 750$ ’ shows a larger width-to-height ratio for the girder cross-section, less thickness for diaphragms and less width for stiffeners around the diaphragm hole, while the case ‘ $[\beta] = 1000$ ’ shows the slender appearance for the girder cross-section which requires three web ribs in the compressive-stress zone and thicker stiffeners for the diaphragm hole to keep local stability. Besides the serious arrangement of stiffeners on the web, the crane made of AL6061 further adds one rib to counter flange local buckling, simultaneously strengthening the diaphragm and its stiffeners to 12 mm.

Comparably, the girder of Q355-steel made crane becomes compact, correspondingly shrinking the flange cantilever only to 110 mm for the trolley railway support.

### 5.2.2 Mechanical Performance

The value enclosed in parenthesis after stress or deformation values denotes the relative deviation from the allowable limit. For the case of Q235 steel with ' $[\beta] = 500$ ', the residual normal and von-Mises stresses in both VI and TI cases are less than 20%, while the residual vertical deformation is up to 45%. This obviously indicates that the design of Q235 steel crane is limited by the strength not stiffness. Therefore, merely adding constraints on the stiffness coefficient will improve the utilization of structural stiffness while maintaining structural strength, as presented in the cases ' $[\beta] = 750$ ' and ' $[\beta] = 1000$ '. Comparably, enhancing the yielding stress from 235 to 355 MPa will produce larger deformations in both vertical and transverse directions, which effectively enhances the utilization of both strength and stiffness, therefore reduces the total mass by a large step. While for the AL6061 case with the same stiffness coefficient, the residuals of normal and von-Mises stresses exceed 45%, while those for deformations are merely 5%. This implies that opposite to Q235 crane, the aluminum-alloy made crane owns a strong large deformable flexibility compared to its strength, becoming the prominent factor to control in crane structural optimization.

### 5.2.3 Mass

Compared to the case of Q235 crane with ' $[\beta] = 500$ ', the ' $[\beta] = 750$ ' case reduces its total mass by 700 kg and the Q355 case even by almost 5 t, where the mass for all stiffeners and end beams accounts for less than 20%. This implies that under the case of less constraint on the stiffness of the crane structure, it is the girder itself, not the stiffeners, mainly shouldering the external loads from goods and trolley. On the other hand, respectively for higher stiffness requirement (' $[\beta] = 1000$ ') or lower strength of material property (AL6061), arrangement on stiffeners is definitely a huge project in terms of web rib number and diaphragm thickness, with the mass of stiffeners and end beams being at least 40%. In this sense, stiffeners make a remarkable contribution to enhancing the structural stiffness.

Related to the mass, the cost at material purchasing period is another concern. Obviously, increasing the yielding stress on steel from Q235 to Q355 will reduce the cost by 17% due to the compact structure of Q355 crane. Besides, under the market setting of 800 USD/ton for steel and 1600 USD/ton for aluminum alloy, it charges a bit more for AL6061 even with half the steel mass compared to Q235 for the same stiffness coefficient. However, noteworthy, under the theory of

full-life cycle design, aluminum-alloy made crane definitely outperforms steel counterparts in multiple aspects: foundation construction, support column building, energy-saving due to lighter weight, and material durability due to corrosion resistance, which hopefully saves thousands of expenses afterward.

## 6 Conclusion

This study explores three optimization methods, namely sub-problem approximation (SPA), sweeping (SW), and first-order (FO) in APDL code, to minimize the mass of an overhead crane girder. The key innovation lies in the real-time adjustment of the number, spacing, location, and dimensions of ribs and diaphragms in each iteration of the optimization process following the girder's cross-section. The optimization model integrates various stresses and deformations from vertical and transverse impact load cases, as well as dynamic vibration frequency, as state variables to achieve the optimal crane mass. Additionally, four intelligent algorithms—Grey Wolf Optimizer, Whale Optimization Algorithm, Particle Swarm Optimization, and Genetic Algorithm—are employed to showcase the superiority of the proposed method. Furthermore, parameter studies are conducted to analyze the impact of stiffness coefficient and material property on the optimized mass of the crane girder. The findings reveal that:

- (1) The optimized girder cross-sections generated by the four intelligent algorithms tend towards a square shape, resulting in stresses or deformations exceeding allowable limits, which are inadequate for bearing vertical loads. In contrast, the optimized girder section obtained through the proposed method (a combination of SPA, SW, and FO through APDL) exhibits a larger height-to-width ratio, with all stresses and deformations from load cases remaining within allowable limits. Thus, the combination of SPA, SW, and FO offers a clear advantage in optimizing girder mass.
- (2) Implementing stricter constraints on vertical deformation in the optimization process enhances the utilization of structural stiffness while maintaining strength for Q235 steel-made cranes. Furthermore, substituting Q235 steel with Q355 steel results in a more compact optimized crane structure, demonstrating improved utilization of both strength and stiffness and consequently leading to a significant reduction in mass. Additionally, adopting aluminum alloy 6061-T6 as the structural material halves the crane's mass compared to steel, albeit at a higher initial purchasing cost due to nearly double the cost per ton. However, buyers are advised to choose aluminum alloy as the material in crane structure due to considerations

including foundation construction, energy efficiency, and material durability within the framework of full-life cycle design.

Future research will focus on a comprehensive analysis of the total cost associated with aluminum alloy crane construction within the context of full-life cycle design, aiming to provide more practical recommendations.

**Funding** This study was funded by the National Natural Science Foundation of China (NSFC) (Grant number: 51978013), the China Scholarship Council (Grant number: 201906545013), the China Post-doctoral Science Foundation (Grant number: 2017M620789), and Beijing University of Technology (Grant numbers: 004000514118567, 004000514119060).

## Declarations

**Conflict of interest** The authors have no competing interests to declare that are relevant to the content of this article.

## References

- Abid, M., Akmal, M., & Wajid, H. (2015). Design optimization of box type girder of an overhead crane. *Iranian Journal of Science and Technology*, *39*, 101–112.
- Alhorani, R. A. M. (2020). Mathematical models for the optimal design of I- and H-shaped crane bridge girders. *Asian Journal of Civil Engineering*, *21*, 707–722.
- Cheng, W. M., Li, Y. M., & Zhang, Z. Q. (2012). Criteria on lightweight design for gantry and overhead cranes. *Chinese Journal of Construction Machinery*, *10*, 41–49.
- Damian, G., & Tomasz, H. (2016). Modelling studies on the use of aluminium alloys in lightweight load-carrying crane structures. *Transport Problems*, *11*, 13–20.
- Deng, Y. S., Fang, B., & Xu, Z. P. (2020). Structure optimization design of gantry crane. *China Heavy Equipment*, *1*, 17–23.
- Fu, W. G., Cheng, W. M., & Yu, L. F. (2013). Bionics design of transverse stiffener in the upright rail box girder based on bamboo structure. *Journal of Southwest Jiaotong University*, *48*, 211–216.
- Hao, F. F., Fan, X. N., & Zhi, B. (2017). Structure and robust optimization design based on additional objective function of the sensitivity. *Journal of Mechanical Strength*, *39*, 1385–1390.
- Hidekazu, N. (2002). First order analysis for automotive body structure design using excel. *R&D Review of Toyota CRDL*, *37*(1), 1–8.
- Hou, H. L., Wang, Z. Y., & Feng, Q. H. (2018). Multi-objective optimization for box girder structure of bridge crane based on sensitivity analysis. *Machine Design and Research*, *34*, 121–125.
- Jarmai, K., Barcsak, C., & Marcsak, G. Z. (2021). A box-girder design using metaheuristic algorithms and mathematical test functions for comparison. *Applied Mechanics*, *2*, 891–910.
- Khoury, G. I. E., Linzell, D. G., & Geschwindner, L. F. (2014). Computational studies of horizontally curved, longitudinally stiffened, plate girder webs in flexure. *Journal of Constructional Steel Research*, *93*, 97–106.
- Khoury, G. I. E., Linzell, D. G., & Geschwindner, L. F. (2016). Flexure-shear interaction influence on curved, plate girder web longitudinal stiffener placement. *Journal of Constructional Steel Research*, *120*, 25–32.
- Kovacs, G., & Farkas, J. (2017). Minimum cost design of overhead crane beam with box section strengthened by CFRP laminates. *Structural Engineering and Mechanics*, *61*, 475–481.
- Li, Y. H., Wang, Z. Y., & Liu, Y. S. (2020). The study on lightweight of the bridge crane girder based on LSTBSVM and bat algorithm. *Machine Design and Manufacturing Engineering*, *49*, 15–49.
- Li, Y., Xiang, D., & Li, Q. W. (2018). Research and application on rapidly lightweight design system of cranes. *Journal of Mechanical Engineering*, *54*, 205–213.
- Pang, F. Z., Jin, Y. Q., & Yao, X. L. (2011). APDL based vibration optimization of a ship foundation. *Advanced Materials Research*, *338*, 525–529.
- Patel, H., Upadhyay, D., & Patel, D. (2020). Design optimization of box girder in gantry crane using finite element analysis software. *International Research Journal of Engineering Technology*, *7*, 1906–1917.
- Pavloviu, G., Savkoviu, M., & Zdravkoviu, N. (2017). Design optimization of the rectangular box section of the double beam bridge crane using Matlab optimization toolbox. In *IX Triennial International Conference* (pp. 37–38).
- Pervan, N., Muminovic, A. J., & Mesic, E. (2020). Dimensional structural mass optimization of a welded I-profile bridge crane girder. *Tehnicki Glasnik*, *14*, 186–193.
- Qi, Q. S., Xu, H., & Xu, G. N. (2021a). Comprehensive research on energy-saving green design scheme of crane structure based on computational intelligence. *AIP Advances*, *11*, 075314.
- Qi, Q., Yu, Y. N., & Qing, D. (2021b). Lightweight and green design of general bridge crane structure based on multi-specular reflection algorithm. *Advances in Mechanical Engineering*, *13*, 1–15.
- Qiu, Y., Yi, P. X., & Nie, F. Q. (2019). Adaptive multi-objective dynamic optimization of the main beam of bridge crane. *Machinery Design and Manufacture*, *11*, 204–208.
- Savkovic, M. M., Bulatovic, R. R., & Gasic, M. M. (2017). Optimization of the box section of the main girder of the single-girder bridge crane by applying biologically inspired algorithms. *Engineering Structures*, *148*, 452–465.
- Su, S., Qin, Y. X., & Yang, K. Y. (2022). Structural optimization of unsymmetrical eccentric load steel box girder based on new swarm intelligence optimization algorithm. *International Journal of Steel Structures*, *22*, 1518–1536.
- Tong, Y. F., Ye, W., & Yang, Z. (2013). Research on multidisciplinary optimization design of bridge crane. *Math Problems in Engineering*. <https://doi.org/10.1155/2013/763545>
- Wan, L., Xu, G. N., & Gu, D. M. (2008). Crane design rule GB/T 3811.
- Wang, J. N., Zhang, Z. W., & Cheng, W. M. (2013). Crane design manual.
- Wang, J. N., & Yu, L. F. (2017). Metal structure of crane transporting mechanism.
- Zhang, Z. W., Wang, J. N., & Cheng, W. M. (2013). Crane design manual.
- Zhang, J., Cheng, W. M., & Li, Y. Q. (2019). Fast and lightweight design of metal structures for gantry cranes with same span and different lifting weights. *Machinery Design and Manufacture*, *S*, 1–4.

- Zhang, H., Qin, Y. X., & Gu, J. P. (2021). Layout optimization of stiffeners in heavy-duty thin-plate box girder. *Ksce Journal of Civil Engineering*, 25, 3075–3083.
- Zhang, J. T., Zhu, H., & Zhao, C. S. (2010). Combined finite element analysis and subproblem approximation method for the design of ultrasonic motors. *Sensors and Actuators a: Physical*, 163(2), 510–515.

Springer Nature or its licensor (e.g. a society or other partner) holds exclusive rights to this article under a publishing agreement with the author(s) or other rightsholder(s); author self-archiving of the accepted manuscript version of this article is solely governed by the terms of such publishing agreement and applicable law.

**Publisher's Note** Springer Nature remains neutral with regard to jurisdictional claims in published maps and institutional affiliations.